

The Tempered Polymerization of Human Neuroserpin

Rosina Noto^{1,9}, Maria Grazia Santangelo^{2,9}, Stefano Ricagno³, Maria Rosalia Mangione¹, Matteo Levantino², Margherita Pezzullo³, Vincenzo Martorana¹, Antonio Cupane², Martino Bolognesi³, Mauro Manno^{1*}

1 Institute of Biophysics, National Research Council of Italy, Palermo, Italy, **2** Department of Physics, University of Palermo, Palermo, Italy, **3** Department of Biomolecular Sciences and Biotechnology, Institute of Biophysics CNR and CIMAINA, University of Milano, Milan, Italy

Abstract

Neuroserpin, a member of the serpin protein superfamily, is an inhibitor of proteolytic activity that is involved in pathologies such as ischemia, Alzheimer's disease, and Familial Encephalopathy with Neuroserpin Inclusion Bodies (FENIB). The latter belongs to a class of conformational diseases, known as serpinopathies, which are related to the aberrant polymerization of serpin mutants. Neuroserpin is known to polymerize, even in its wild type form, under thermal stress. Here, we study the mechanism of neuroserpin polymerization over a wide range of temperatures by different techniques. Our experiments show how the onset of polymerization is dependent on the formation of an intermediate monomeric conformer, which then associates with a native monomer to yield a dimeric species. After the formation of small polymers, the aggregation proceeds via monomer addition as well as polymer-polymer association. No further secondary mechanism takes place up to very high temperatures, thus resulting in the formation of neuroserpin linear polymeric chains. Most interesting, the overall aggregation is tuned by the co-occurrence of monomer inactivation (i.e. the formation of latent neuroserpin) and by a mechanism of fragmentation. The polymerization kinetics exhibit a unique modulation of the average mass and size of polymers, which might suggest synchronization among the different processes involved. Thus, fragmentation would control and temper the aggregation process, instead of enhancing it, as typically observed (e.g.) for amyloid fibrillation.

Citation: Noto R, Santangelo MG, Ricagno S, Mangione MR, Levantino M, et al. (2012) The Tempered Polymerization of Human Neuroserpin. *PLoS ONE* 7(3): e32444. doi:10.1371/journal.pone.0032444

Editor: Piero Andrea Temussi, Università di Napoli Federico II, Italy

Received: October 18, 2011; **Accepted:** January 31, 2012; **Published:** March 6, 2012

Copyright: © 2012 Noto et al. This is an open-access article distributed under the terms of the Creative Commons Attribution License, which permits unrestricted use, distribution, and reproduction in any medium, provided the original author and source are credited.

Funding: SR MP and MB acknowledge the financial support from Fondazione Cariplo, Milano, Italy (NOBEL project Transcriptomics and Proteomics Approaches to Diseases of High Socio-medical Impact: a Technology Integrated Network), from the Italian MIUR (Ministero dell'Istruzione, dell'Università e della Ricerca) (Bando Futuro in Ricerca [FIRB] contract RBLA03B3KC_005) and by the financial support of Telethon – Italy (Grant no. GGP11057). The funders had no role in study design, data collection and analysis, decision to publish, or preparation of the manuscript.

Competing Interests: The authors have declared that no competing interests exist.

* E-mail: mauro.manno@cnr.it

⁹ These authors contributed equally to this work.

Introduction

Serpins (SERine Protease INhibitor) are highly conserved proteins that control serine protease activities in different extracellular environments [1]. Several mutations identified in humans are at the origin of a large class of pathologies, known as serpinopathies, which share a common molecular mechanism: the polymerization of a mutant serpin and its accumulation within the endoplasmic reticulum (ER) [2]. Such event causes toxicity (gain of function phenotype) in the tissue producing the mutant serpin, or the lack of protease inhibition in the proper extracellular environment (loss of function phenotype). Serpins are composed of three β -sheets (A–C) and an exposed mobile reactive centre loop (RCL), acting as a target for the serine protease [3]. The protease cleaves the RCL triggering the insertion of the RCL into the A β -sheet as a strand; however, the protease remains covalently trapped, almost irreversibly, as an acyl enzyme intermediate [4]. The mechanism of serpin polymerization is intimately related to their inhibitory function [5,6]. Indeed, unlike other globular proteins, native serpins are folded in a metastable conformation, and reach a more stable state by interlocking the RCL into the A β -sheet, thus reducing its mobility [7]. This is achieved upon RCL cleavage, or by adopting a distorted conformation in which the

RCL is fully or partially inserted into the A β -sheet without cleavage (latent conformation) [8]. Alternatively, the RCL may be inserted into the sheet of a neighbor serpin molecule thus forming dimers and eventually polymers [9]. For these characteristics, serpin polymers are ordered structures, which do not require extensive protein unfolding and, in general, do not activate the unfolded protein response or other stress signaling pathways from the ER [10]. This marks the peculiarity of serpinopathies within the larger class of protein conformational diseases, which include important disorders such as amyloidoses and other neurodegenerative diseases [11].

Here, we study the mechanism of polymerization of human neuroserpin (NS), a secretory protein produced mainly in neurons, playing a role in axonogenesis and in regulating synaptic plasticity through the inhibition of tissue-type plasminogen activator (tPA) [6,12,13]. It is also associated to Alzheimer's disease through a still not clear role [14,15]. NS is related to the autosomal dominant dementia Familial Encephalopathy with Neuroserpin Inclusion Bodies (FENIB) [16]. Selected point mutations promote NS polymerization [17–19] and its ER retention, with a high genotype-phenotype correlation [20], thus providing a clear example of how serpin polymerization causes human disease [21,22]. Beyond its clinical relevance, NS is a suitable model for

biophysical studies of serpin polymerization due to its close structural homology with the archetypal serpin α 1-antitrypsin (AAT) [23], whose deficiency represents the most common serpinopathy [24], but also due to its capability of forming polymers by thermal stress [17,25,26] or under acidic conditions [27], even in its wild-type form.

The classical model for serpin polymerization [9], understood for the Z variant of AAT, foresees the formation of an intermediate state in the pathway to polymerization [8,28], which can accept the insertion of the RCL from a neighbor serpin molecule forming “loop-sheet” polymers [29]. The same mechanism is likely responsible for the formation of loop-sheet polymers of other mutant variants of AAT [30–32], and NS [15,26]. However, an alternative serpin polymerization mechanism has been proposed, based on the crystal structure of a closed dimer of antithrombin grown under acidic conditions. In this model, polymers would form by iterative domain swapping of a hairpin composed by strands s4A and s5A [33]. A more recent crystallographic study revealed alternative domain swapping involved in the structure of an antitrypsin trimer [34]. Although the relevance of this model for the polymerization *in vivo* is not clear yet, it suggests that different environmental conditions and specific point mutations may lead to structurally diverse polymers, through polymerization mechanisms that are still a matter of debate. Detailed knowledge of serpin structural behavior (intermediate conformations, conversion to latency, polymerization) is fundamental for the design of therapeutic aids helping prevent diseases associated with serpin polymerization.

NS forms polymeric structures upon heating above physiological temperatures [17]. As shown by our previous work [25,26], neuroserpin maintains a folded conformation and polymerogenic properties up to high temperatures, even if the molecular structure of polymeric and latent conformers may be slightly different above 80°C. In the present work, we study the mechanism of polymerization of human neuroserpin at different temperatures and concentrations by static and dynamic light scattering (LS) and size exclusion chromatography (SEC), two techniques suitable for monitoring the mass and size evolution of protein aggregates, as well as by intrinsic tryptophan photoluminescence (PL) to reveal the conformational changes occurring during aggregation. Our experiments, in keeping with previous results [15,26], confirm that the polymerization is rate limited by two processes: activation of an intermediate, and dimerization of such an intermediate with a native monomer. Moreover, our data show that the late stage of aggregation is dominated not only by the process of monomer addition to polymers, but also by polymer-polymer association. Interestingly, we observe a remarkable correlation between the hydrodynamic radius and the mass of polymers, which highlights the supramolecular structure of NS aggregates as polymeric chains formed only by end-to-end association, and not by other secondary mechanisms, such as branching or lateral association. The same processes seem to operate in a large range of temperatures.

The most striking observation emerging from our experiments is a modulation in the growth of the polymer mass and size with time, which implies the occurrence of fragmentation, or any kind of depolymerization such as simple monomer release from polymers, in keeping with analogous observation for AAT polymerization [35]. This behavior is quite unique in the scenario of protein aggregation. For example, in the case of amyloid fibrillation, aggregation is typically enhanced by fragmentation [36]. The analogy with the oscillations in the length of microtubules prompted us to consider some kind of synchronization or feedback among the different processes involved [37].

However, a rationale for such a re-entrant growth can be found qualitatively by assuming the occurrence of depolymerization below a given polymer size, and the concomitant process of latentization that sequesters the active monomers thus tempering the progression of aggregation. The idea of a fragile interlocking of the RCL in the polymeric structures, prompted by our observation of a fragmentation mechanism, finds a counterpart in the lack of stability of the NS-tPA complex. Indeed, contrary to other serpins, NS is a transient inhibitor of tPA and the acyl-enzyme NS-tPA complexes are short-lived, [23,38]. The fragility of both polymers and complexes may be related to the relative stability of the different neuroserpin conformers, and may be relevant both for the pathology and for the physiological role of NS.

Results

Kinetics of polymerization studied by LS

Simultaneous dynamic and static LS measurements were performed at different temperatures from 37 to 85°C, at concentrations around 4.5 μ M (except above 70°C, where the concentration was reduced down to 1.5 μ M). Fig. 1 shows typical intensity autocorrelation functions measured at selected times during polymerization at 45°C. The intensity autocorrelation functions in the course of the kinetics were fit by both a regularization scheme and a double exponential function, in order to derive the hydrodynamic radii R_h of monomeric and polymeric species, as reported in the Methods section [39–41]. The z-average hydrodynamic radius has been also calculated by the robust cumulant method [42]. All the fitting procedures yield perfectly consistent results. Data in Fig. 1 indicate the increase of the polymeric fraction accompanied by a time dependent increase of the polymer hydrodynamic radius, that reaches a value of $R_h \sim 15$ nm after 960 minutes of incubation at 45°C. Upon incubation at high temperature, neuroserpin forms polymers up to a hydrodynamic radius of a few tens of nanometers, in agreement with Transmission Electron Microscopy images (data not shown. See also Fig. S1) [25].

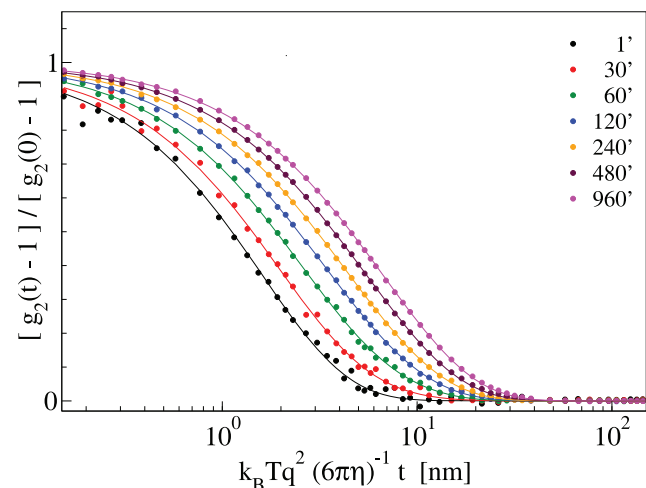


Figure 1. Intensity autocorrelation function $g_2(t)$ of a 8.5 μ M NS solution during polymerization at 45°C at selected times, as shown in the legend (coloured circles), and the relative fit by exponential functions (solid curve). The time axis is renormalized by the following thermodynamic and experimental quantities: q is the scattering vector, T the temperature, k_B the Boltzmann constant, and η the solvent viscosity.

doi:10.1371/journal.pone.0032444.g001

Fig. 2 displays the time evolution of the distribution functions $P(R_h)$ of the hydrodynamic radii R_h at different temperatures. The $P(R_h)$ values in the figure were color-coded so that the red color denotes the most frequent R_h of the population. In the intermediate range of temperatures we clearly note that the distribution functions $P(R_h)$ are mainly bimodal, and composed of one monomer peak and one polymer peak. The polymer fraction grows uniformly with a variance essentially proportional to the average. In other words, the distribution of polymer hydrodynamic radii $P(R_h)$ shifts to larger R_h without changing its shape on a logarithmic scale and thus exhibits a self-similar shape in the course of the kinetics.

The kinetics at high temperature deserves specific attention (Figs. 2k, 2l). At 85°C polymerization takes place in a few minutes leading to the formation of micron-sized aggregates, as already reported in our previous work [25]. At later stage, the diffusion of such aggregates is affected by their large-size and entanglement, as observed in jammed polymer networks [43] (Fig. S2). A detailed study of this late stage is beyond the scope of the present work. Here, it is worth to remark that the aggregation in the early stage (i.e. that occurring in the first 10÷30 minutes) is akin to that occurring at lower temperatures and leading to the formation of serpin-like polymers.

Occurrence of different processes: latentization, monomer addition, fragmentation and polymer-polymer association

It is worth noting that in the polymerization kinetics (Fig. 2) a residual fraction of monomeric species is maintained even after the formation of protein aggregates, as clearly seen up to 57°C. A mechanism that prevents monomer depletion is related to the inactivation of neuroserpin monomers due to the formation of latent conformers (latentization), both at low and high temperatures [15,25].

From the static scattering intensity, one obtains the weight average mass M_w of protein aggregates. Fig. 3a shows the kinetics of M_w at the various temperatures, and Fig. 3b shows the z-averaged hydrodynamic radii in the same conditions. The kinetics of polymerization exhibits two stages: an initial fast formation of small polymeric species, growing in mass and size, is followed by the aggregation of larger polymers with a lower rate. These two stages are not clearly separated at the lower temperatures, while they can be clearly recognized above 50°C.

In the intermediate range of temperatures, we observe a peculiar behavior at the transition between the two stages. The signal related to M_w and R_h is not a monotonous function of time, but follows a modulated, pseudo-oscillatory behavior. At temperatures around 55°C, a reduction of the average mass and size is evident, implying the fragmentation or depolymerization of polymer aggregates (Figs. 2 and 3a,b). The above polymerization feature is observed at 55°C at different protein concentrations, with a concentration-dependent characteristic time (Fig. 4). At 55°C, the quasi-oscillatory behavior and the presence of fragmentation is even more striking than at the other temperatures.

The average mass and hydrodynamic radius continue growing even at the late stage (Figs. 2, 3, 4). In general, if the aggregation by monomer addition were not preceded by nucleation or activation, the polymer mass could grow only to a value which is less or equal to three times the initial value [44]. In Figs. 3 and 4, we may recognize at long times an asymptotic power-law behavior in the growth of polymer mass and size: $M_w \sim t^z$ and $R_h \sim t^{z/d}$. By simultaneous inspection of the curves at different temperatures, the best exponent turns out to be $z = 2/3$. This indicates that polymerization proceeds not only by monomer addition but also by polymer-polymer association (or fragmentation). Indeed, if only dimerization and monomer addition took place, the weight average mass would reach a stationary value due to monomer consumption. Chiou et al. assigned the larger rate of association to

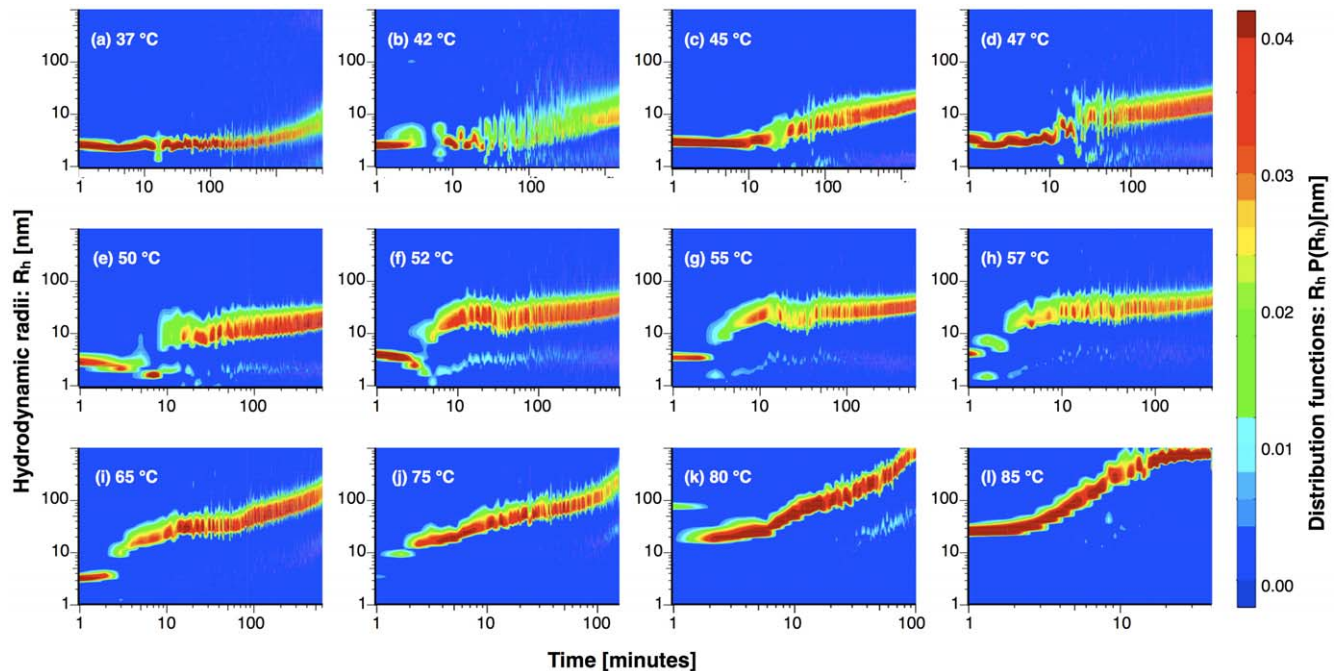


Figure 2. Distribution functions of hydrodynamic radii versus incubation time at different temperatures (as specified in each panel).

doi:10.1371/journal.pone.0032444.g002

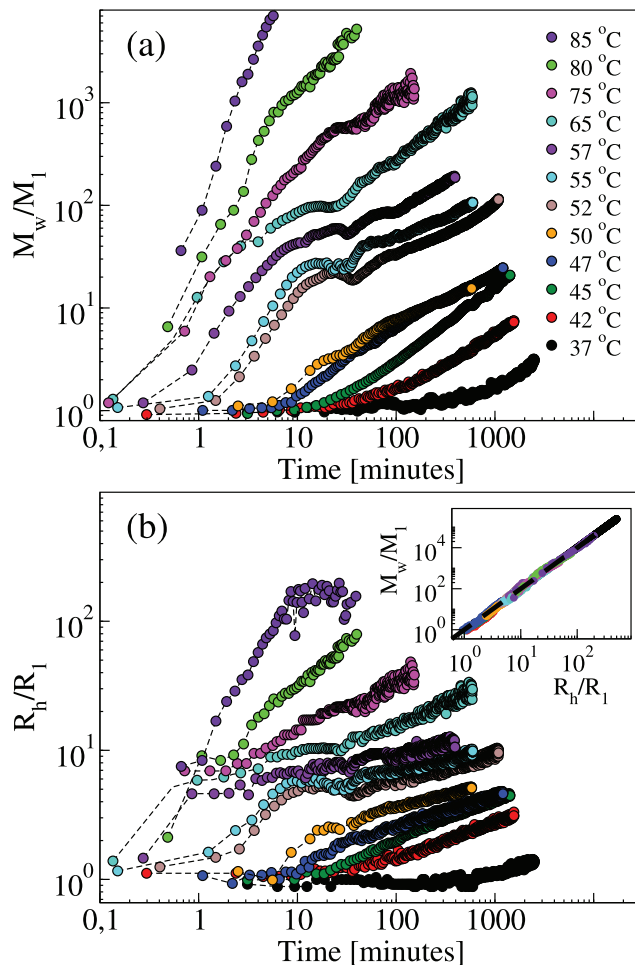


Figure 3. Kinetics of neuroserpin polymerization at different temperatures. (a) Weight average mass M_w normalized by the monomer mass M_1 . (b) z-average hydrodynamic radius R_h normalized by the monomer radius R_1 . Inset: Correlation between M_w and R_h ; the dashed line is a power law with exponent 2. doi:10.1371/journal.pone.0032444.g003

the dimerization process and considered polymer-polymer association as negligible [15]. Those results are based on single molecule fluorescence experiments, and therefore they are intrinsically sensitive to the low molecular mass species, while our experiments based on LS are sensitive to larger species. Thus, we may consider that the data reported here and by Chiou et al. are not incompatible: they simply reflect a different focus on large and small aggregates, respectively.

Neuroserpin forms random polymers, with no secondary mechanism

The growths of M_w and R_h are correlated, as shown in the inset of Figs. 3b and 4b. The two quantities are related by a power-law: $M_w/M_1 = (R_h/R_1)^d$, where $M_1 = 46$ kDa and $R_1 = 3$ nm are respectively the molecular mass and the hydrodynamic radius of neuroserpin monomers, and the exponent $d = 2 \pm 0.1$ is the apparent fractal dimension, a parameter related to the packing and self-similarity of aggregates. For instance, the value $d = 2$ is typical of random polymers, as expected in the present case [45]. Interestingly, the same type of correlation extends over all kinetics and at all temperatures and concentrations. Therefore, the same type of structure is formed with no secondary aggregation

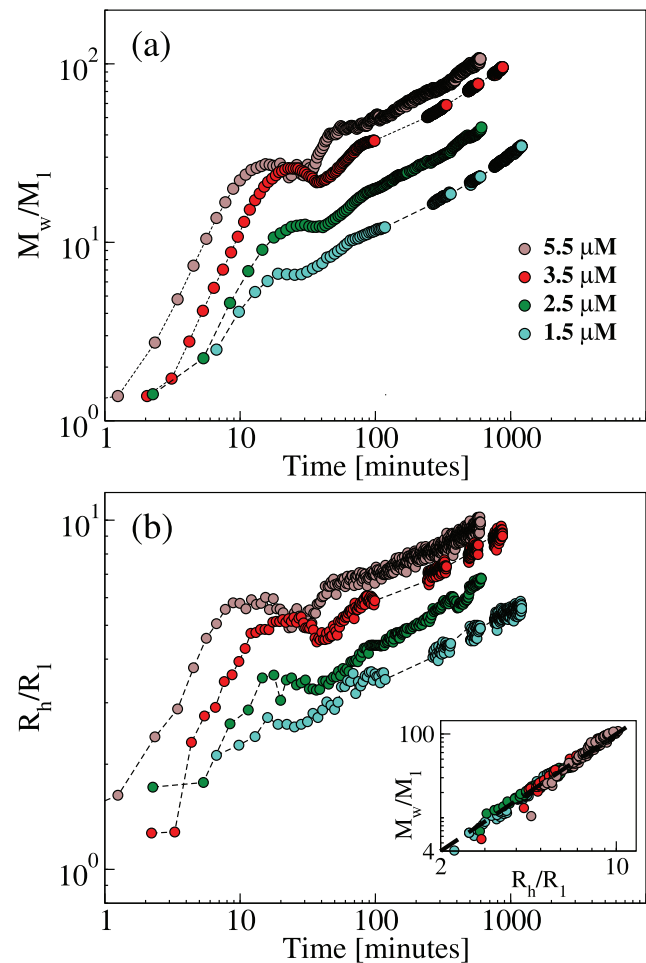


Figure 4. Kinetics of neuroserpin polymerization at 55°C and at different concentrations. (a) Weight average mass M_w normalized by the monomer mass M_1 . (b) z-average hydrodynamic radius R_h normalized by the monomer radius R_1 . Inset: Correlation between M_w and R_h ; the dashed line is a power law with exponent 2. doi:10.1371/journal.pone.0032444.g004

mechanisms, such as lateral association [46], branching [47], or secondary nucleation [48,49]. It is worth noting that the power-law starts from the monomer size, which may be considered the building unit of polymer structures. In other words, the persistence length of polymers is of the order of the monomer size, in keeping with TEM images (Fig. S1).

Kinetics of polymerization by SEC

LS measurements are intrinsically more sensitive to molecules and aggregates with a higher molecular mass. In order to confirm the kinetics results reported above with a focus on the monomer and small polymers, we performed time-lapse SEC experiments. The inset of Fig. 5 displays the chromatographic profiles of samples incubated at 55°C. The corresponding percent amounts of monomers, dimers and polymers are reported in Fig. 5. These results confirm the persistence of the monomeric fraction, as obtained in the analysis of LS data. At about one hour of incubation we observe a temporary reduction of the polymeric fraction, which is then restored to higher values. Such a reduction occurs immediately after the initial main increase of the polymeric populations, which coincides with the first stage of the kinetics observed by LS. This is an independent confirmation of the

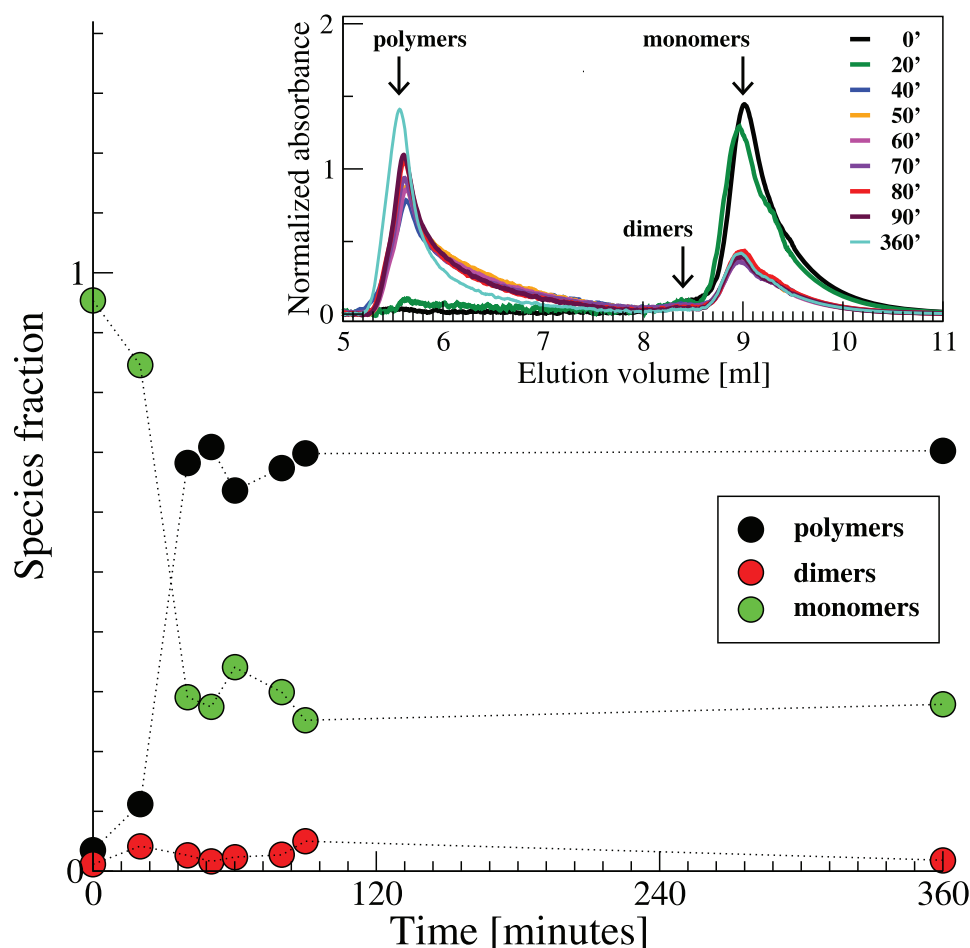


Figure 5. Kinetics of neuroserpin polymerization at 55°C monitored by time-lapse SEC: fraction of monomeric (green circles), dimeric (red circles) and polymeric (black circles) species. Inset: Chromatograms at different times upon incubation at 55°C.
doi:10.1371/journal.pone.0032444.g005

existence of a fragmentation mechanism, which complements the more statistically significant LS experiments. Further, it evidences that the fragmentation includes not only a break of extended polymers but also monomer release from polymers.

Kinetics of polymerization by tryptophan PL

The association of molecules into polymers implies a change in the native conformation. In order to monitor such a change, we measured PL spectra during the kinetics at 37, 45, 55, and 65°C (Figs. 6a, b, c, d). During polymerization the tryptophan luminescence band exhibits a progressive red shift. Accordingly, the signal intensity decreases, probably due to the thermal activation of non-radiative channels, which quench the luminescence from the excited electronic state. Fig. 6e shows the results of the first moment analysis on the steady-state PL of neuroserpin tryptophans. In general, a structureless red-shifted band in tryptophan PL points to a polar environment [50]; for example, a red-shift is observed in protein thermal unfolding [51]. Neuroserpin has three tryptophans, at positions 279, 190 and 154. The latter is on the F helix, which is likely to play a relevant role in the polymerization mechanism and to move in order to leave space for the RLC insertion into β -sheet A [52]. Thus, the formation of an active intermediate and the subsequent association may be reasonably related to a more solvent exposed Trp154 residue. Here, we observe that the shift is complete within the first

stage of kinetics, that is while the process of activation and dimer formation is prevalent. No large conformational changes occur at a later stage, which is therefore dominated by the association of already formed polymers.

Discussion

“Universal” features of NS polymerization

Even if the polymerization kinetics exhibits a certain level of complexity, one may estimate the initial rate of polymer growth, as well as the final association rate, and gain some insight on the general physical mechanisms underlying the reported NS polymerization kinetics. To this purpose, a double phenomenological scaling of LS data was performed to match both the initial and the long-time asymptotic part of the kinetics at each temperature and concentration. The time axis was rescaled by using a characteristic time τ . An effective amplitude parameter a was used to rescale the polymer mass in excess with respect to monomer, that is the quantity $M_w/M_1 - 1$. The resulting plot is reported in Fig. 7 and shows that the initial and final stages of the measured polymerization kinetics obey some general (“universal”) behavior.

The curve that best describes the initial mass growth is a quadratic law, with the form: $M_w/M_1 - 1 = \frac{1}{2} \omega^2 t^2$, where the rate $\omega = [1/(\alpha\tau^2)]^{1/2}$, related to the scaling parameters, depends upon

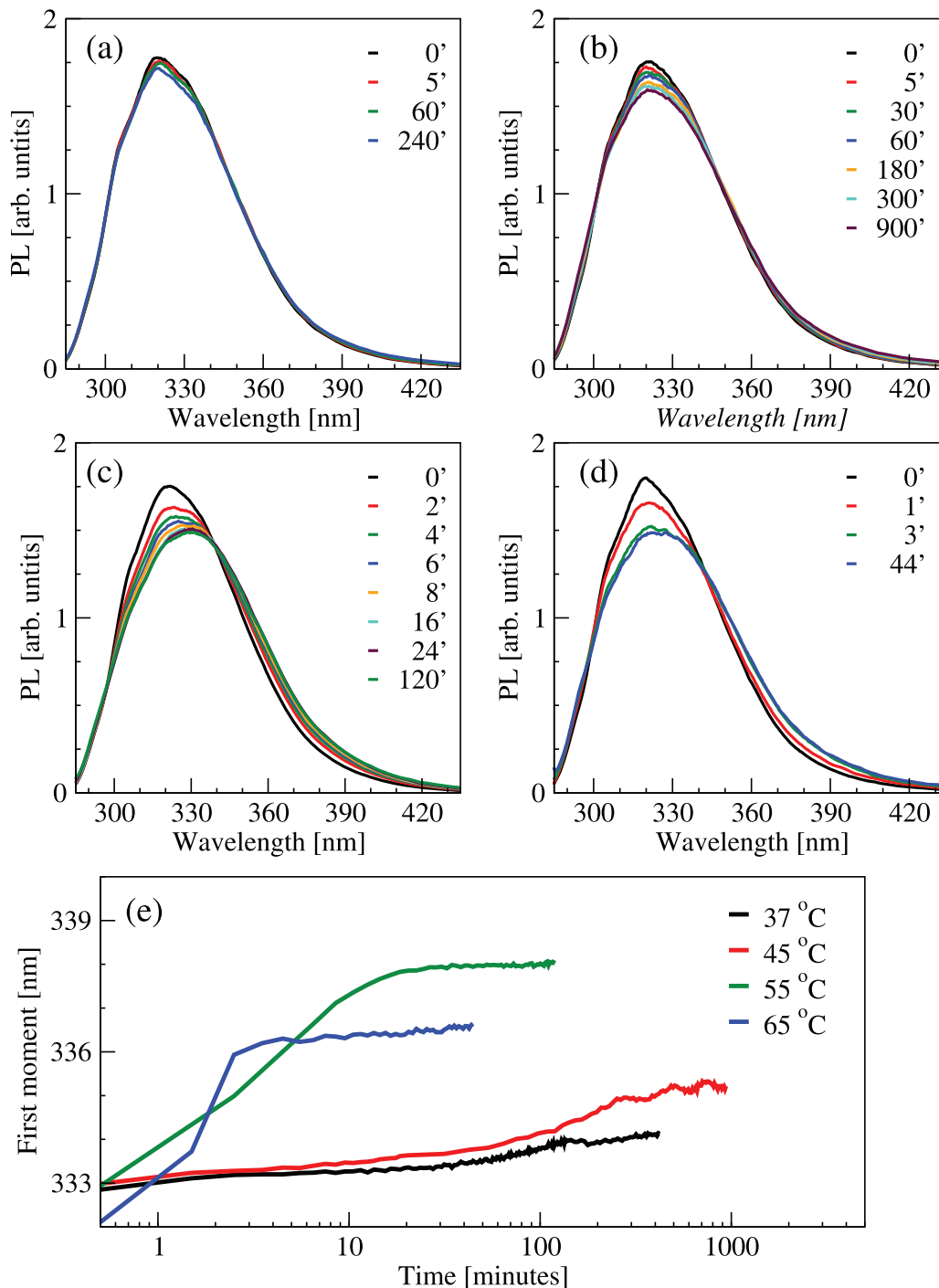


Figure 6. Kinetics of neuroserpin polymerization monitored by time-lapse PL. (a–d) Emission spectra during the kinetics at 37°C, 45°C, 55°C, 65°C. (e) Kinetics of the first moment of the emission bands in the previous panels. doi:10.1371/journal.pone.0032444.g006

temperature and concentration. The latter expression may be considered as an expansion at time zero of M_w/M_n , where the first time derivative is zero and the second one is ω^2 . In the classical model by Oosawa and coworkers [53] and in the subsequent extensions [54], the initial growth of the aggregate concentration with a power-law with an exponent $n+1$ implies that the aggregation is initiated by the formation of a nucleus of n monomers. Roberts and collaborators have extended this scheme

by including a reversible conformational transition preceding nucleation [55]. In the present case, the initial quadratic growth of data in Fig. 7 implies that the initial polymerization stage is dominated by the sequence of two processes: a monomer conformational transition (the activation process) with a rate κ_A and a dimerization process between a native and an activated monomer with a concentration-dependent rate $c\kappa_D$, where c is the molar concentration. Indeed, if the initial growth were due to the

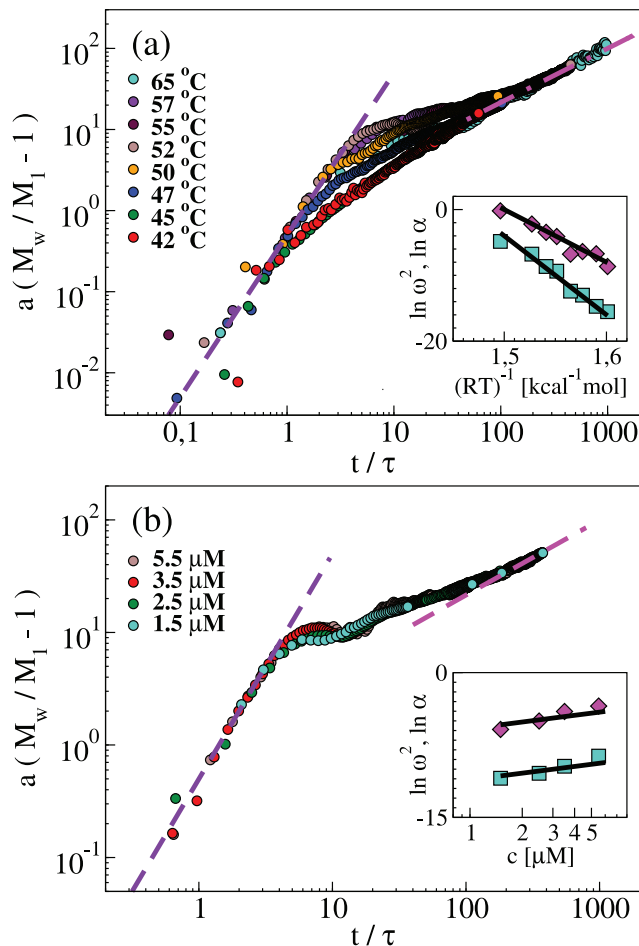


Figure 7. Kinetics of neuroserpin polymerization at different temperatures (panel a) and concentrations (panel b). Weight average mass from figs. 3a and 4a, respectively, rescaled as explained in the main text. Insets: Kinetics rates obtained from the scaling parameters ω^2 (squares) and α (diamonds). doi:10.1371/journal.pone.0032444.g007

association of two native monomers, the weight averaged mass would have a non-null first-derivative at time zero, and hence a linear growth [41,54]. On the other hand, if two activated monomers were required to initiate polymerization, a higher power-law behavior (namely t^3) would have been observed. Therefore, the quadratic behavior of the onset of aggregation is a further endorsement of the dimerization between a native and an activated monomer [15]. The set of equations, which describes the processes involved in polymerization, along with the expansion at time zero, is reported as Supporting Information (Tables S1, S2).

The second time-derivative of M_w/M_1 is given by the product of the rates of two processes $\omega^2 = 2\kappa_A\kappa_D c$. The linear concentration dependence of the parameter ω^2 at 55°C is estimated in the inset of Fig. 7b. One obtains: $\kappa_A\kappa_D = 8 \text{ s}^{-2} \text{ M}^{-1}$. The parameter ω has been calculated at different temperatures, and it is shown in an Arrhenius plot in the inset of Fig. 7a. This indicates that the same processes operate in this range of temperatures. One obtains an enthalpy change for the activation and dimerization of 120 kcal mol⁻¹. If we take this result and extrapolate at 45°C we obtain a value $\kappa_A\kappa_D = 0.02 \text{ s}^{-2} \text{ M}^{-1}$, which is one order of magnitude lower than the value estimated by Chiou et al. [15]. Again, this discrepancy can be rationalized by considering the different

sensitivity to polymer size, which may bias both their data and our data in opposite directions.

Beyond the growth at low incubation times, we may rationalize also the behavior at very long incubation times. Indeed, the average size of polymers has a limited and constant polydispersity (Fig. 2), and the curves of the weight average mass tend asymptotically to a power-law. In Fig. 7, the second phenomenological scaling was performed in order to report the asymptotic behavior of each curve to the power-law $t^{2/3}$. With these features, we may argue that the association rate has a mass dependence, which is a homogeneous function of mass with an exponent λ [56]. Such condition typically occurs when the aggregation mechanism is limited by diffusion [57], so that λ is the reciprocal of the scaling exponent between aggregate mass and hydrodynamic radius: $\lambda = -d^{-1}$ [44]. In such a case the analytical solution for the weight average mass is: $M_w/M_1 \sim (\alpha t)^z$, where $z^{-1} = 1 - \lambda$. In the present case, we find $d = 2$ (insets of Fig. 3b and 4b), and $z = 2/3$ (Fig. 7) that consistently imply $\lambda = -0.5$. The same type of growth would be found if the fragmentation kernel were also a homogeneous function. In such a case the structure of the kernel is less straightforwardly related to aggregate properties [58]. However, the same type of power-law may be found asymptotically under given conditions [59]. In order to obtain a not stationary solution, as in the present case, the breakup rate at large cluster size should be overwhelmed by the rate of polymer-polymer association.

The rate α may be estimated by the scaling parameters of Fig. 7: $\alpha = \omega a^{-1}$. Its concentration dependence at 55°C is shown in the inset of Fig. 7b. One obtains $\alpha/c = 3000 \text{ s}^{-1} \text{ M}^{-1}$. The same parameter, obtained at different temperatures, can be drawn in an Arrhenius plot as in the inset of Fig. 7a. The enthalpy change related to this parameter, derived from the slope of the Arrhenius plot, is 80 kcal mol⁻¹. By extrapolating this result to 45°C we obtain a value $\alpha = 55 \text{ s}^{-1}$, which is close to the value obtained by Chiou et al. for a rate of association [15]. Indeed, the parameter α represents a generic affinity rate, since it is not only related to the association mechanism but also in a hidden way to the fragmentation. Although its physical meaning is not clearly worked out, it is clearly related to the energy of activation of all the processes prevalent at the late stage of aggregation and mainly to that of polymer-polymer association.

Kinetics of different processes: a clue from basic models

Our experiments allow extending the kinetic scheme of neuroserpin polymerization, by taking into account the different processes involved. The early stages of aggregation are rate-limited by two processes: (i) the activation of monomers, with a rate κ_A , through a conformational change that allows them to initiate the polymerization and (ii) the formation of dimers, with a rate κ_D , by the association of a native with an activated monomer. The elongation of polymeric structure proceeds beyond dimerization by two other processes: (iii) the addition of monomers to already formed polymers, with a rate κ_M and (iv) the association of polymers of different lengths, with a rate κ_P . The latter process has been first clearly observed in the present work for NS aggregation. The main new qualitative feature added by the results here reported is represented by the occurrence of a modulation, and sometimes a decrease, of the polymer mass and size. Such consideration implies the introduction of an additional process, (v) polymer fragmentation, with a rate κ_F . In the case of neuroserpin we know that a further process takes place, i.e. (vi) the formation of latent monomers, with a rate κ_L .

A general kinetic scheme accounting for all the above processes can be built to produce numerical profiles of experimental available quantities (e.g. scattered intensity). As a matter of fact,

only a few model parameters can be set on the basis of our experimental results, and more details should be known to aim at a quantitative fitting of the data. However, a lot can be learned from a basic model, which is able to spot qualitatively the general features of the polymerization kinetics. In the following we sketch the role of the different processes involved by calculating the growth of the weight average mass for given values of the rates. The complete kinetic scheme of equations used is reported as Supporting Information (Table S2). In such an example, we take equal value for the rates of the three processes of activation, dimerization and monomer addition ($\kappa_A = \kappa_D = \kappa_M = 1$).

In Fig. 8a, we show qualitatively the effects of including polymer-polymer association in the overall aggregation process. The kinetics of weight average mass M_w are plotted for different values of the rate κ_P of polymer-polymer association. As recalled above, in the absence of polymer-polymer association ($\kappa_P = 0$,

dotted curve in Fig. 8a) M_w reaches a plateau due to monomer depletion. The increase of the association rate κ_P causes M_w to increase. In this example the increase is linear as a function of time, since we used for simplicity a constant size-independent rate. A more realistic representation would require a size-dependent rate, as discussed above, yielding an asymptotic power-law with a sub-linear growth.

The other process required by our experiments is polymer fragmentation. Indeed, monomer release from polymers is suggested by our experiments (Fig. 5), while it is not clear yet whether other types of polymer breakdown are occurring. From the observation of the small polydispersity in the distribution of hydrodynamic radii (Fig. 2), we may argue that the fragmentation rate should be a smooth function of polymer size, if not a homogeneous function (as discussed above). Another possibility would be that fragmentation is restricted to a given size of

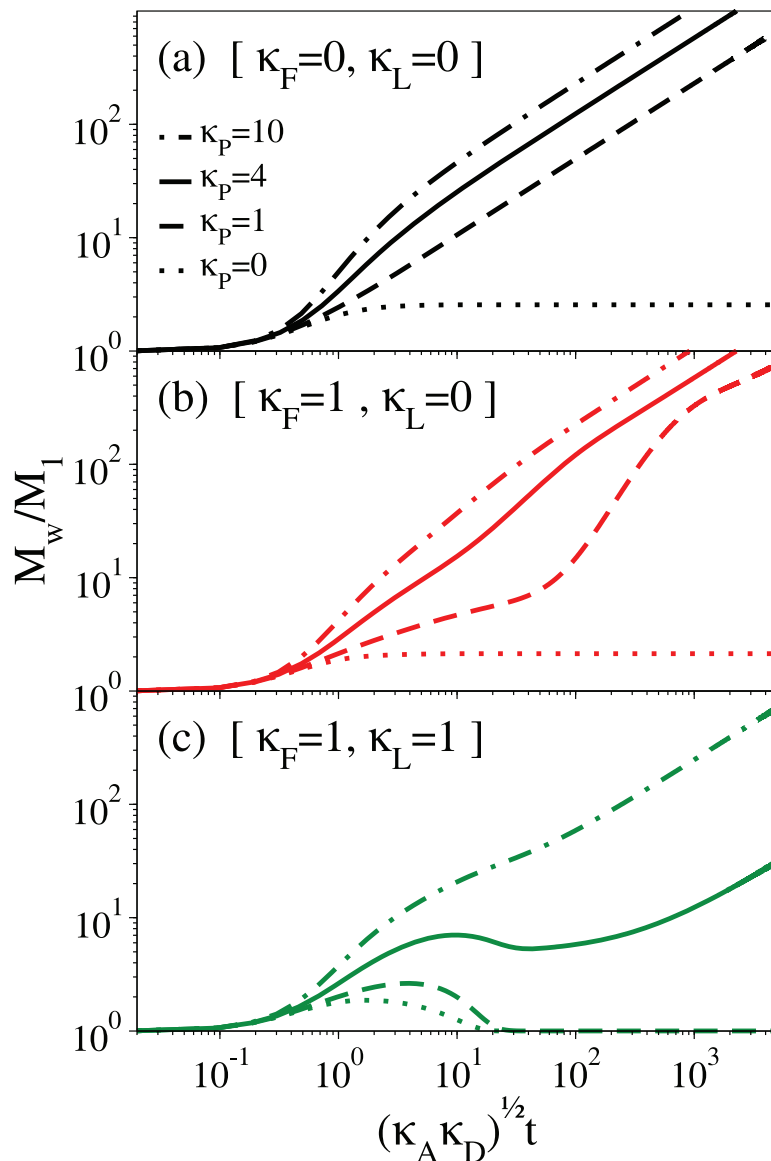


Figure 8. Polymerization kinetics due to different processes. The y-axis displays the weight average mass, the x-axis displays the time normalized by using the rates of activation (κ_A) and dimerization (κ_D). (a) Kinetics at different rates of polymer-polymer association (κ_P). (b) Kinetics as in the previous panel by addition of a fragmentation process from polymers below 31 units. (c) Kinetics as in the previous panel by addition of a latentization process from activated monomers.

doi:10.1371/journal.pone.0032444.g008

polymers. This possibility is particularly sound since it naturally introduces a separation of the time-scales of fragmentation and polymer-polymer association even if they share similar rates. In Fig. 8b, we show the kinetics of M_w at different rates of polymer-polymer association calculated by including the release of monomers from polymers of size below 31 units, and with a rate $\kappa_P = \kappa_M = 1$. While in the absence of polymer-polymer association M_w reaches a stationary value ($\kappa_P = 0$, dotted curve in Fig. 8b), the plateau is lost due to the prevalence of association at a later stage, and M_w grows with a sizeable modulation of the slope, especially for smaller values of κ_P .

Last, we consider the effect of the other process peculiar to serpin polymerization, which is the latentization. We calculated the kinetics of M_w by including latentization from the active monomers, as suggested in ref. [15], with a rate $\kappa_L = \kappa_M = 1$. The results for different rates of polymer-polymer association are shown in the curves of Fig. 8c. We note that when such association is suppressed ($\kappa_P = 0$) the latent monomer acts as a sink with respect to the other species, since latentization was assumed to be irreversible. For given values of the association rates ($\kappa_P = 4$ in the example shown in Fig. 8), the co-occurrence of fragmentation and latentization determines a transient reduction of the weight average mass, which resembles qualitatively our experimental findings. Indeed, after the activated formation of dimers and small polymers, fragmentation preserves the amount of monomeric species that are then sequestered by latentization. At later time polymer-polymer association becomes overwhelming and sustain a monotonous growth of the average mass.

This scheme, pictorially described in Fig. 9, is able to capture the main qualitative features of our experimental data, as shown by the continuous curve in Fig. 8c. However, it is still not complete to fit quantitatively the overall kinetics. We are not aware of any alternative models explaining the details of such a unique aggregation process.

It is of some interest to compare our observations of NS polymerization with analogous features reported for different aggregating macromolecular systems. In particular, the phenomenon of aggregate fragmentation is faced in the literature of

amyloid fibrils. In such a field, the effect of fragmentation in general is linked to an increase of amyloid toxicity and enhancement of fibrillation due to the fact that more active ends become available for elongation [36,47].

The modulated increase of neuroserpin polymer mass is reminiscent of another physiologically important case, which is the growth and oscillation of microtubules [37]. The growth of microtubules is controlled by ATP hydrolysis, via a cycle of processes: (i) active ATP-tubulins form active ATP-polymers, (ii) active ATP-polymers turn into inactive ADP-polymers, (iii) the latter undergo depolymerization and release ADP-tubulin, (iv) ADP-tubulin is activated to ATP-tubulin to restart the cycle [60]. The synchronization of these processes, under particular protein and ATP concentrations, generates sustained oscillations in microtubule length. In the present case, we are only facing a modulation of the signal and a pseudo-oscillatory behavior at the crossover between two kinetic stages. Note also that the available models for microtubule oscillation succeed in reproducing experimental data only by introducing some kind of concentration-dependent rate in one of the processes involved [60–62]. On the contrary, based on what has been reported here, we may conclude that the basic model of polymerization, based on the first order processes of activation, latentization and fragmentation and the second order processes of monomer and polymer association, is not sufficient and some other “ingredient” is missing. We have shown that an interesting hint comes from an ad hoc kernel built to allow the fragmentation only of polymers of a specific size. Further advancements may take into account more complex phenomena. However, this would require more detailed experimental data on polymer structure, and it is therefore left for future studies.

It is worth noting that the proposed polymerization scheme (Fig. 9) implicitly supports the classical “loop-sheet” model for serpin polymerization [9]. Indeed, the occurrence of a fragmentation process, including the release of active monomers, adequately fits with a model, which does not foresee an extensive unfolding of proteins assembled into polymers, as (*e.g.*) in the “loop-sheet” model.

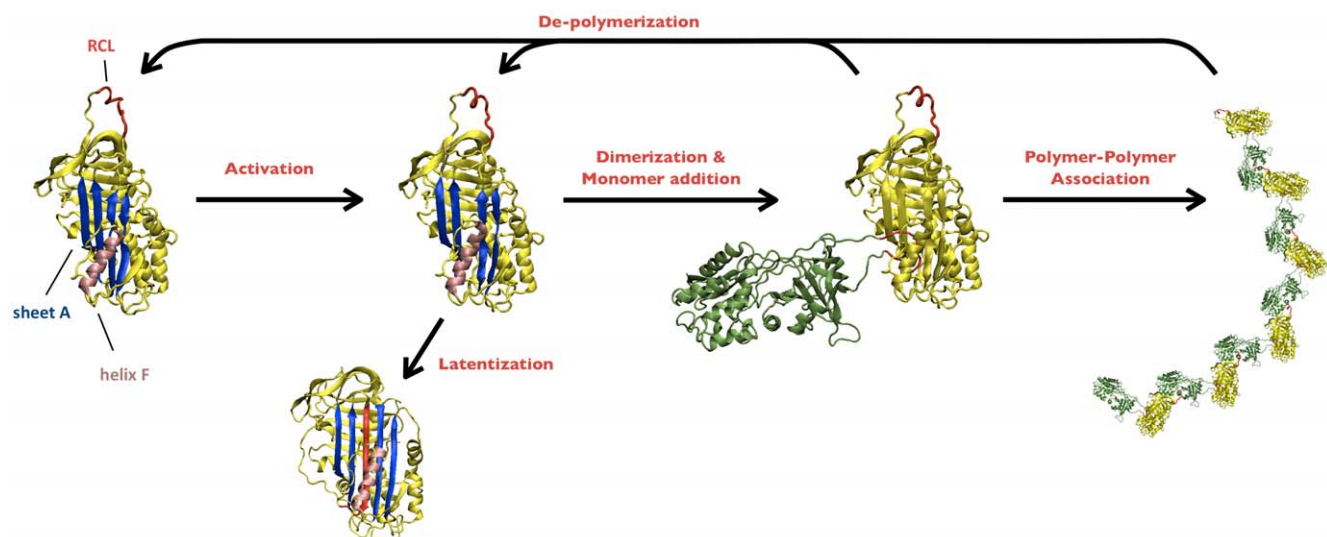


Figure 9. Scheme of neuroserpin polymerization. The arrows and the text highlight the different processes involved. The small bars on the structure of the native protein (left) point to the main structural features of neuroserpin discussed for the polymerization process: the reactive center loop (RCL), the β -sheet A and the α -helix F. doi:10.1371/journal.pone.0032444.g009

Conclusive remarks

The polymerization of human neuroserpin was studied at different temperatures and concentrations. Our experiments show that linear polymeric chains are formed in a wide range of temperatures above the physiological one, with no other secondary mechanism (Figs. 2, 3, 4).

At the early stage of kinetics, the polymerization is driven by the process of activation of a monomeric intermediate conformer, prone to aggregation, and by the process of NS dimerization. The occurrence of these two processes had been already observed in a previous work [15], and it is here confirmed and characterized as the onset of the overall aggregation process. Then polymerization proceeds both by monomer addition to polymers and by polymer-polymer association. The latter process was revealed by the experiments here presented and was found to be diffusion-limited, at least in the late stage.

The most interesting observation emerging from our data is that NS polymerization is tempered by the occurrence of a fragmentation mechanism that likely also involves monomer release from polymers. Such a process is unique in the panorama of protein aggregation, where the most typical effect of fragmentation is an enhancement of the growth of aggregates. Moreover, the modulation of aggregate mass suggests a synchronization of the processes involved, in analogy with the observations on microtubule formation. A possible explanation of the observed modulation in the growth of neuroserpin polymers was found by the occurrence of latentization, that is the formation of inactive monomers, and the existence of relatively small fragile polymers.

The interplay among different process can thus provide a rationale for our experimental observation. We believe that some ingredient is still missing from the proposed model in order to expand the context of classical aggregation scheme. Further studies on the structure of neuroserpin polymers and latent monomers will help obtaining a quantitative explanation of the well-tempered aggregation of human neuroserpin.

Materials and Methods

Sample preparation

Recombinant NS was expressed and purified according to a previously published protocol [23]. The lack of cleaved NS was checked by gel electrophoresis (data not shown). A stock solution of a few mg/ml was prepared in 50 mM KCl, 10 mM HCl-Tris buffer pH 7.4, and stored at -80°C . The stock solution was diluted to the final concentration, aliquoted and kept at 4°C for a few days before experiments. Each aliquot was accurately filtered through Anatop 20 nm syringe-filters to remove large or small aggregates. The lack of aggregates was carefully checked by dynamic LS [39]. Protein concentration was measured by UV absorption at 280 nm (extinction coefficient: $0.803\text{ cm}^{-1}\text{ mg}^{-1}\text{ ml}^{-1}$). All chemicals were of reagent grade.

Large Angle LS

Time-resolved dynamic LS experiments were performed at different temperatures. Samples were placed in a thermostated cell compartment of a Brookhaven Instruments BI200-SM goniometer, equipped with a solid-state laser tuned at $\lambda_0 = 532\text{ nm}$. The temperature was controlled within 0.05°C with a thermostated recirculating bath. Scattered light intensity and its time autocorrelation function $g_2(t)$ were measured simultaneously by using a Brookhaven BI-9000 correlator. Correlation functions $g_2(t)$ were analyzed by using a constrained regularization method in order to determine the distribution $P(R)$ of the hydrodynamic radii R :

$g_2(t) = 1 + |P(R) \exp\{-D(R)q^2t\} dR|^2$. In the last expression, $q = 4\pi\tilde{n}\lambda_0^{-1}\sin(\vartheta/2)$ is the scattering vector, with ϑ being the scattering angle and \tilde{n} the medium refractive index, and $D(R)$ is the diffusion coefficient, related to R by the Stokes-Einstein relation: $D(R) = (k_B T)/(6\pi\eta R)$, where k_B is the Boltzmann constant, T is the temperature and η is the solvent viscosity [40]. Alternatively $g_2(t)$ were analyzed by fitting with a bimodal distribution function containing the monomer hydrodynamic radius R_1 and the z-averaged polymer hydrodynamic radius R_p , $g_2(t) = 1 + |A_1 \exp\{-D(R_1)q^2t\} + A_p \exp\{-D(R_p)q^2t\}|^2$, where A_1 and A_p are the scattering amplitude related to the two contributions. From data analysis, one obtains the z-average hydrodynamic radius R_h , which is defined as the harmonic average of the radii of the different species: $R_h^{-1} = \int P(R)R^{-1} dR$. Absolute values for scattered intensity (Rayleigh ratio) were obtained by normalization with respect to toluene, whose Rayleigh ratio at 532 nm was taken as $28 \cdot 10^{-6}\text{ cm}^{-1}$. From the Rayleigh ratio $R(q)$, at a given scattering vector q , one obtains the weight average mass M_w of species in solution: $R(q) = HcM_w P(q)$, where c is the total mass concentration, $P(q)$ is the average form factor and $H = [2\pi\tilde{n} d\tilde{n}/dc \lambda_0^{-2}]^2 N_A^{-1}$ is a constant which depends upon the Avogadro number N_A , the incident wavelength λ_0 , the refractive index of the medium \tilde{n} and the refractive index increment $d\tilde{n}/dc$. The latter was assumed to be $0.18\text{ cm}^3\text{ g}^{-1}$, a typical value for protein physiological solutions. The average form factor at 90° was computed by using the Guinier approximation, which holds for objects with a size small with respect to the inverse of the scattering vector: $P(q) = [1 + 1/3(qR_g)^2]^{-1}$, where R_g is the ratio of gyration. We estimated R_g from the measured z-average hydrodynamic radius ($R_g = R_h$), which is a well-taken approximation for protein oligomers in solution [39]. As a matter of fact, for most of our experiments the form factor $P(q)$ is essentially not relevant due to the moderate size of the objects in solution.

Steady state PL

Steady state PL measurements were performed by incubating $4.5\text{ }\mu\text{M}$ NS samples in a quartz cuvette with a 3 mm optical path, in a thermostated cell holder of a Jasco FP-6500 spectrofluorimeter. The temperature was controlled within 0.05°C with a thermostated recirculating bath. The PL emission bands were measured with a 280 nm excitation wavelength, 3 nm excitation and emission bandwidth, 100 nm min^{-1} scan-speed, and 2 s response. The first momentum M_1 of the emission band was calculated as $M_1 = hc \int [E L(E)dE]^{-1}$, where $L(E)$ is the normalized luminescence spectral profile at emission energy E , h is the Planck constant and c is the speed of light.

Time lapsed SEC

Aggregate mass percentage was measured by SEC using a Phenomenex BioSep (SEC-S3000, $300 \times 7.80\text{ mm}$) column (Amersham) connected to a HPLC device (LC-2010 AT Prominence, Shimadzu, Kyoto, Japan), equipped with a UV-vis photodiode array detector and a $50\text{ }\mu\text{L}$ sample loop. Samples of $4.5\text{ }\mu\text{M}$ neuroserpin solution were incubated at 55°C for various time intervals in thermostated bath and directly transferred to the HPLC system. The samples were eluted at a flow of 0.8 mL min^{-1} in the sample buffer and absorption was measured at 280 nm. The percentage of monomers, dimers and larger polymers was estimated from the area of the related peaks with respect to the total area of eluate. The polymer, dimer and monomer peaks are taken within a range of elution volume of 5.0 to 8.1 ml, 8.1 to 8.6 ml and 8.6 ml to 12.0 ml, respectively.

Supporting Information

Figure S1 Transmission electron microscopy of neuroserpin polymers. Polymers were formed by incubation of 0.5 mg ml⁻¹ neuroserpin solutions overnight at 45°C (panel a) and for 2 hours at 85°C (panel b). A 10 μL aliquot was adsorbed on 200 mesh formvar/carbon grids for 5 minutes, washed with distilled water and negatively stained with 2% uranyl acetate. Imaging was obtained by a EFTEM Leo912 ab (Zeiss, Oberkochen, Germany) transmission electron microscope at 80 kV, equipped with Proscan 1K slowscan CCD. (TIF)

Figure S2 Neuroserpin polymerization at 85°C. (a) Intensity autocorrelation functions at selected times during polymerization of a 1.5 mM neuroserpin solution at 85°C. (b) Kinetics of weight average mass M_w (black), z-average hydrodynamic radius R_h (red), characteristic time τ_{slow} (blue) and intensity I_{slow} (green) related to the slow decay. The polymer size increases in a few minutes from 85 nm to 500 nm. Afterwards, a second relaxation process appears in the intensity autocorrelation functions. This relaxation cannot be ascribed to a diffusional process and it was described by fitting with a compressed exponential function with exponent 2 and a characteristic time $t_{slow} = 200 \pm 25$ ms. The correlation function were fit using the following expression: $g_2(t) = 1 + |A_p \exp\{-D(R_p/q)^2 t\} + A_{slow} \exp\{-[t/t_{slow}]^2\}|^2$. The amplitude and the characteristic time of such a slow process are reported in the next panel. The nature of this process is not clear. By considering analogous findings in gelling colloidal systems we may speculate that it is related to the constrained motion of large entangled or jammed polymer networks, as noted in the main text. (PDF)

References

- Silverman GA, Bird PI, Carrell RW, Church FC, Coughlin PB, et al. (2001) The serpins are an expanding superfamily of structurally similar but functionally diverse proteins. Evolution, novel functions, mechanism of inhibition and a revised nomenclature. *J Biol Chem* 276: 33293–33296.
- Goputu B, Lomas DA (2009) Conformational pathology of the serpins: themes, variations and therapeutic strategies. *Annu Rev Biochem* 78: 147–176.
- Gettins PGW (2002) Serpin Structure, Mechanism, and Function. *Chem Rev* 102: 4751–4803.
- Huntington JA, Read RJ, Carrell RW (2000) Structure of a serpin-protease complex shows inhibition by deformation. *Nature* 407: 923–926.
- Whistock JC, Bottomley SP (2006) Molecular gymnastic: serpin structure, folding and misfolding. *Curr Opin Struct Biol* 16: 761–768.
- Caccia S, Ricagno S, Bolognesi M (2010) Molecular bases of neuroserpin function and pathology. *BioMol Concepts* 1: 117–130.
- Cabrita LD, Bottomley SP (2004) How do proteins avoid becoming too stable? Biophysical studies into metastable proteins. *Eur Biophys J* 33: 83–88.
- Goputu B, Hazes B, Chang WSW, Dafforn TR, Carrell RW, et al. (2000) Inactive conformation of the serpin α_1 -antichymotrypsin indicates two-stage insertion of the reactive loop: Implications for inhibitory function and conformational disease. *Proc Natl Acad Sci USA* 97: 67–72.
- Lomas DA, Evans DL, Finch JT, Carrell RW (1992) The mechanism of Z α_1 -antitrypsin accumulation in the liver. *Nature* 357: 605–607.
- Davies MJ, Miranda E, Rousset BD, Kaufman RJ, Marciniak SJ, et al. (2009) Neuroserpin Polymers Activate NFB by a Calcium Signaling Pathway That Is Independent of the Unfolded Protein Response. *J Biol Chem* 284: 18202–18209.
- Carrell RW, Lomas DA (1997) Conformational disease. *The Lancet* 350: 134–138.
- Hastings GA, Coleman TA, Haudenschild CC, Stefansson S, Smith EP, et al. (1997) Neuroserpin, a brain-associated inhibitor of tissue plasminogen activator is localized primarily in neurons. *J Biol Chem* 272: 33062–33067.
- Miranda E, Lomas DA (2006) Neuroserpin: a serpin to think about. *Cell Mol Life Sci* 63: 709–722.
- Kinghorn KJ, Crowther DC, Sharp LK, Nerelius C, Davis RL, et al. (2006) Neuroserpin binds A β and is a neuroprotective component of amyloid plaques in Alzheimer disease. *J Biol Chem* 281: 29268–29277.
- Chiou A, Hagglof P, Orte A, Chen AY, Dunne PD, et al. (2009) Probing neuroserpin polymerization and interaction with amyloid- β peptides using single molecule fluorescence. *Biophys J* 97: 2306–2315.
- Davis RL, Shrimpton AE, Holohan PD, Bradshaw C, Feiglin D, et al. (1999) Familial dementia caused by polymerization of mutant neuroserpin. *Nature* 401: 376–379.
- Belorgey D, Crowther DC, Mahadeva R, Lomas DA (2002) Mutant neuroserpin (Ser49Pro) that causes the familial dementia FENIB is a poor proteinase inhibitor and readily forms polymers in vitro. *J Biol Chem* 277: 17367–17373.
- Belorgey D, Sharp LK, Crowther DC, Onda M, Johansson J, et al. (2004) Neuroserpin Portland (Ser52Arg) is trapped as an inactive intermediate that rapidly forms polymers: implications for the epilepsy seen in the dementia FENIB. *Eur J Biochem* 71: 3360–3367.
- Onda M, Belorgey D, Sharp LK, Lomas DA (2005) Latent S49P neuroserpin forms polymers in the dementia familial encephalopathy with neuroserpin inclusion bodies. *J Biol Chem* 280: 13735–13741.
- Davis RL, Shrimpton AE, Carrell RW, Lomas DA, Gerhard L, et al. (2002) Association between conformational mutations in neuroserpin and onset and severity of dementia. *Lancet* 359: 2242–2247.
- Miranda E, Romisch K, Lomas DA (2004) Mutants of neuroserpin that cause dementia accumulate as polymers within the endoplasmic reticulum. *J Biol Chem* 279: 28283–28291.
- Miranda E, MacLeod I, Davies MJ, Perez J, Romisch K, et al. (2008) The intracellular accumulation of polymeric neuroserpin explains the severity of the dementia FENIB. *Hum Mol Genet* 17: 1527–1539.
- Ricagno S, Caccia S, Sorrentino G, Antonini G, Bolognesi M (2009) Human Neuroserpin: Structure and Time-Dependent Inhibition. *J Mol Biol* 388: 109–121.
- Carrell RW, Lomas DA (2002) α_1 -antitrypsin deficiency - A model for conformational diseases. *Nature* 407: 923–926.
- Ricagno S, Pezzullo M, Barbiroli A, Manno M, Levantino M, et al. (2010) Two Latent and Two Hyperstable Polymeric Forms of Human Neuroserpin. *Biophys J* 99: 3402–3411.
- Santangelo MG, Noto R, Levantino M, Cupane A, Ricagno S, et al. (2012) On the molecular structure of neuroserpin polymers. *Proteins* 80: 8–13.

Table S1 Kinetic scheme for neuroserpin polymerization. The different molecular species and the different processes involved are listed, along with their rates. (PDF)

Table S2 Kinetic scheme for neuroserpin polymerization. This set of equations describes the time evolution of monomeric and polymeric species. The last equation describes the time evolution of the experimentally accessible weight average mass M_w , which is proportional to the second moment of the distribution of molecular species. The short notations defined in Table S1 are used, along with the notation $O(t^3)$ standing for terms of the order of t^3 or higher. This general scheme was used to generate the curves of Fig. 8, by using the following expressions: $\kappa_A = 1$, $\kappa_D = 1$, $\kappa_R = \kappa_F$, $\kappa_{L*} = \kappa_{L*}^* = 0$, $a_{Np} = 1$, $a_{Ip} = 0$, $a_{NI} = 1$, $a_{II} = 0$, $b_{Ip} = 0$, $b_{NN} = b_{II} = b_{NI} = 0$, $b_{Np} = 1$ for $p < 32$, and $b_{Np} = 0$ for $p > 31$. (PDF)

Acknowledgments

We thank S. Caccia, D. A. Lomas and E. Miranda for helpful discussions. We also thank N. Santo (Centro Interdipartimentale di Microscopia Avanzata, University of Milan, Milan, Italy) for technical support; A. Emanuele and P. L. San Biagio for close collaboration and support. We are in debt with C. J. Roberts for his hints and the critical discussion of the kinetic model.

Author Contributions

Conceived and designed the experiments: RN SR ML VM AC MB MM. Performed the experiments: RN MGS MRM VM MM. Analyzed the data: MGS MRM VM MM. Contributed reagents/materials/analysis tools: AC MB. Wrote the paper: MM. Designed the software used in analysis: VM. Lead for protein production and purification: SR MP MB. Assisted with manuscript design: RN MGS SR ML VM AC.

27. Belorgey D, Hagglof P, Onda M, Lomas DA (2010) pH dependent stability of neuroserpin is mediated by histidines 119 and 138; Implications for the control of β -sheet A and polymerization. *Methods* 53: 255–266.
28. Dafforn TR, Mahadeva R, Elliott PR, Sivasothy P, Lomas DA (1999) A kinetic mechanism for the polymerization of α_1 -antitrypsin. *J Biol Chem* 274: 9548–9555.
29. Sivasothy P, Dafforn TR, Gettins PGW, Lomas DA (2000) Pathogenic α_1 -Antitrypsin Polymers Are Formed by Reactive Loop- β -Sheet A Linkage. *J Biol Chem* 275: 33663–33668.
30. Miranda E, Perez J, Ekeowa UI, Hadzic N, Kalsheker N, et al. (2010) Conformational specificity of polymers of α_1 -antitrypsin that are associated with liver disease. *Hepatology* 52: 1078–1088.
31. Ekeowa UI, Freeke J, Miranda E, Gooptu B, Bush MF, et al. (2010) Defining the mechanism of polymerization in the serpinopathies. *Proc Natl Acad Sci USA* 107: 17146–17151.
32. Tsutsui Y, Kuri B, Sengupta T, Wintrode PL (2008) The structural basis of serpin polymerization studied by hydrogen/deuterium exchange and mass spectrometry. *J Biol Chem* 283: 30804–30811.
33. Yamasaki M, Li W, Johnson DJ, Huntington JA (2008) Crystal structure of a stable dimer reveals the molecular basis of serpin polymerization. *Nature* 455: 1255–1258.
34. Yamasaki M, Sendall TJ, Pearce MC, Whisstock JC, Huntington JA (2011) Molecular basis of α_1 -antitrypsin deficiency revealed by the structure of a domain-swapped trimer. *EMBO reports* 12: 1011–1017.
35. Purkayastha P, Klemke JW, Lavender S, Oyola R, Cooperman BS, et al. (2005) α_1 -Antitrypsin Polymerization: A fluorescence Correlation Spectroscopy Study. *Biochemistry* 44: 2642–2649.
36. Xue WF, Hellewell AL, Gosal WS, Homans SW, Hewitt EW, et al. (2009) Fibril Fragmentation Enhances Amyloid Cytotoxicity. *J Biol Chem* 284: 34272–34282.
37. Carlier MF, Melki R, Pantaloni D, Hill TL, Chen Y (1987) Synchronous oscillations in microtubule polymerization. *Proc Natl Acad Sci USA* 84: 5257–5261.
38. Barker-Carlson K, Lawrence DA, Schwartz BS (2002) Acyl-Enzyme Complexes between Tissue-type Plasminogen Activator and Neuroserpin are Short-Lived in Vitro. *J Biol Chem* 277: 46852–46857.
39. Manno M, Craparo EF, Martorana V, Bulone D, San Biagio PL (2006) Kinetics of insulin aggregation: Disentanglement of amyloid fibrillation from large-size cluster formation. *Biophys J* 90: 4585–4591.
40. Berne BJ, Pecora R (1976) *Dynamic Light Scattering*. New York: Wiley-Interscience.
41. Carrota R, Manno M, Giordano FM, Longo A, Portale G, et al. (2009) Protein stability modulated by a conformational effector: effects of trifluoroethanol on bovine serum albumin. *Phys Chem Chem Phys* 11: 4007–4018.
42. Frisken BJ (2001) Revisiting the method of cumulants for the analysis of dynamic light-scattering data. *Appl Opt* 40: 4087–4091.
43. Cipelletti L, Manley S, Ball RC, Weitz DA (2000) Universal Aging Features in the Restructuring of Fractal Colloidal Gels. *Phys Rev Lett* 84: 2275–2278.
44. Carrota R, Manno M, Bulone D, Martorana V, San Biagio PL (2005) Protofibril Formation of Amyloid β -Protein at Low pH via a Noncooperative Elongation Mechanism. *J Biol Chem* 280: 30001–30008.
45. de Gennes PG (1979) *Scaling Concepts in Polymer Physics*. Ithaca and London: Cornell University Press.
46. Manno M, Craparo EF, Podestà A, Bulone D, Carrota R, et al. (2007) Kinetics of Different Processes in Human Insulin Amyloid Formation. *J Mol Biol* 366: 258–274.
47. Andersen CB, Yagi H, Manno M, Martorana V, Ban T, et al. (2009) Branching in Amyloid Fibril Growth. *Biophys J* 96: 1529–1536.
48. Ferrone F (1999) Analysis of protein aggregation kinetics. In: Wetzel R, ed. *Methods in Enzymology*. San Diego: Elsevier Academic Press. pp 256–274.
49. Knowles TPJ, Waudby CA, Devlin GL, Cohen SIA, Aguzzi A, et al. (2009) An Analytical Solution to the Kinetics of Breakable Filament Assembly. *Science* 326: 1533–1537.
50. Lakowicz JR (1999) *Principles of Fluorescence Spectroscopy*. New York: Kluwer Academic/Plenum Publishers.
51. D'Amico M, Raccosta S, Cannas M, Martorana V, Manno M (2011) Existence of Metastable Intermediate Lysozyme Conformation Highlights the Role of Alcohols in Altering Protein Stability. *J Phys Chem B* 115: 4078–4087.
52. Krishnan B, Gierasch LM (2011) Dynamic local unfolding in the serpin α_1 antitrypsin provides a mechanism for loop insertion and polymerization. *Nature Struct Mol Biol* 18: 222–227.
53. Oosawa F, Asakura S (1975) *Thermodynamics of the Polymerization of Proteins*. London: Academic Press.
54. Flyvbjerg H, Jobs E, Leibler S (1996) Kinetics of self-assembling microtubules: An inverse problem in biochemistry. *Proc Natl Acad Sci USA* 93: 5975–5979.
55. Andrews JM, Roberts CJ (2007) A Lumry-Eyring Nucleated Polymerization Model of Protein Aggregation Kinetics: 1. Aggregation with Pre-Equilibrated Unfolding. *J Phys Chem B* 111: 7897–7913.
56. Taylor TW, Sorensen CM (1987) Moment analysis of the cluster-size-distribution approach to scaling during coagulation. *Phys Rev A* 36: 5415–5419.
57. Olivier BJ, Sorensen CM (1990) Variable aggregation rates in colloidal gold: Kernel homogeneity dependence on aggregant concentration. *Phys Rev A* 41: 2093–2100.
58. Vigil RD, Ziff RM (1989) On the Stability of Coagulation-Fragmentation Population Balances. *J Colloid Interface Sci* 133: 257–264.
59. Sorensen CM, Zhang HX, Taylor TW (1987) Cluster-Size Evolution on a Coagulation-Fragmentation System. *Phys Rev Lett* 59: 363–366.
60. Chen Y, Hill TL (1987) Theoretical studies oscillations in microtubule polymerization. *Proc Natl Acad Sci USA* 84: 8419–8423.
61. Marx A, Mandelkow E (1994) A model of microtubule oscillations. *Eur Biophys J* 22: 405–421.
62. Jobs E, Wolf DE, Flyvbjerg H (1997) Modeling Microtubule Oscillation. *Phys Rev Lett* 79: 519–522.